Mon. Not. R. Astron. Soc. **000**, 000–000 (1993)

ASCA observations of Deep ROSAT fields - II. The 2–10 keV AGN luminosity function

B.J.Boyle[1], I.Georgantopoulos[2], A.J.Blair[2], G.C.Stewart[2], R.E.Griffiths[3], T.Shanks[4], K.F.Gunn[4], O.Almaini[5]

[1] *Anglo-Australian Observatory, PO Box 296, Epping, NSW 2121, Australia*
[2] *Department of Physics & Astronomy, The University of Leicester, Leicester LE1 7RH*
[3] *Department of Physics, Carnegie Mellon University, Wean Hall, 5000 Forbes Ave., Pittsburgh, PA 15213, USA*
[4] *Physics Department, University of Durham, South Road, Durham DH1 3LE*
[5] *Institute of Astronomy, Madingley Road, Cambridge CB3 0HA*

ABSTRACT

We present additional optical spectroscopic identifications of sources identified in three deep *ASCA* GIS fields which also form part of a deep *ROSAT* survey. In total, 26 *ASCA* sources have been detected down to a 2-10 keV flux limit of $S_{2-10} = 5 \times 10^{-14}\,\mathrm{erg\,cm^{-2}\,s^{-1}}$. LDSS observations have increased the spectroscopic completeness of the survey to between 65 and 85 per cent, with identifications for up to 13 QSOs with broad emission lines and 6 objects with narrow emission lines. Combining these objects with the AGN identified in the *HEAO 1* sample by Grossan, we find evidence for significant cosmological evolution in the 2-10 keV band ($\langle \frac{V_e}{V_a} \rangle = 0.63 \pm 0.03$), fit by a pure luminosity evolution model; $L \propto (1+z)^k$, $k = 2.04^{+0.16}_{-0.22}$. The present-epoch 2-10 keV AGN X-ray luminosity function, $\Phi(L_X)$, is best represented by a two power law function: $\Phi(L_X) \propto L^{-3.0}$, $L^* > 10^{44.1}\,\mathrm{erg\,s^{-1}}$; $\Phi(L_X) \propto L^{-1.9}$, $L^* < 10^{44.1}\,\mathrm{erg\,s^{-1}}$. Depending on the extent to which we extrapolate the $z = 0$ AGN luminosity function, we predict a total contribution to the 2-10 keV X-ray background from QSOs and narrow-emission-line galaxies which ranges from 48 per cent (for AGN with $L_X > 10^{42}\,\mathrm{erg\,s^{-1}}$) to 80 per cent ($L_X > 10^{39}\,\mathrm{erg\,s^{-1}}$).

Key words: X-rays: general – galaxies: active – quasars: general

1 INTRODUCTION

The *ROSAT* mission has provided us with a significant advance in our knowledge regarding the nature of the faint X-ray source population at soft 0.5-2 keV energies. Deep *ROSAT* pointings have resolved over half of the soft X-ray background (Hasinger et al. 1993) and numerous spectroscopic studies of the optical counterparts to these sources (Shanks et al. 1991, Carballo et al. 1995, Georgantopoulos et al. 1996, Bower et al. 1996) have shown that the sources are predominantly QSOs and narrow-emission-line galaxies.

In contrast, until recently, little has been known about the nature of the X-ray source population at harder energies (> 2 keV), where the bulk of the energy in the X-ray background (XRB) lies (see Fabian and Barcons 1992). The *HEAO 1* A-1 experiment (Wood et al. 1984) resolved less than 5 per cent of the 2-10 keV X-ray background at its flux limit $S_{2-10} \sim 5 \times 10^{-12}\,\mathrm{erg\,cm^{-2}\,s^{-1}}$.

Data obtained with the *ASCA* satellite now allows us to extend this limiting flux by a factor of almost 100, affording a new insight into the nature of the faint X-ray source population in the 2-10 keV energy range. In a previous paper in this series (Georgantopoulos et al. 1997, hereinafter Paper I), we reported on *ASCA* observations of three fields we had previously studied with *ROSAT*. The limiting flux for the *ASCA* survey was $S_{2-10} \sim 5 \times 10^{-14}\,\mathrm{erg\,cm^{-2}\,s^{-1}}$, resolving approximately 30 per cent of the 2-10 keV background. By cross-correlating the positions of the *ASCA* sources with the *ROSAT* sources, we were able to derive optical identifications for approximately half of the *ASCA* sources. However, there were too few identifications to yield a definitive answer as to the nature of the majority of the objects in the *ASCA* source list. We have therefore attempted to obtain further spectroscopic identifications for the optical counterparts in our *ASCA* source list in order to obtain a clearer picture of the nature of the faint 2-10 keV X-ray source population. In section 2 we describe our optical and X-ray observations and present an analysis of the source populations identified in section 3. We discuss in section 4 the implications for the 2-10 keV background and we present our conclusions in section 5. Values of $H_0 = 50\,\mathrm{km\,s^{-1}\,Mpc^{-1}}$ and $q_0 = 0.5$ are assumed throughout this paper. All co-ordinates are given in equinox J2000.0.

2 OBSERVATIONS

2.1 X-ray

Full details of the X-ray observations for the three *ASCA* GIS fields used in this study are reported in Paper I. Briefly, three fields; GSGP4 ($00^{\rm h}57^m25.2^s$ $-27^\circ37'48''$), QSF3 ($03^{\rm h}41^m44.4^s$ $-44^\circ07'05''$), F855 ($10^{\rm h}46^m24.0^s$ $-00^\circ20'38''$), in the deep *ROSAT* survey of Shanks et al. (in preparation) were observed with the *ASCA* GIS for total exposure times up to 218 ksec. We detected 26 sources down to a 4σ threshold. A total of $1\,{\rm deg}^2$ was searched to a mean flux limit of $S_{2-10} \sim 5 \times 10^{-14}\,{\rm erg\,cm^{-2}\,s^{-1}}$.

Although the Point Spread Function (PSF) of the *ASCA* GIS leads to relatively poor positional accuracy (1σ error $\sim$ 1 arcmin) for the detected sources, we were able to cross-correlate the *ASCA* source catalogue on these three fields with our deep 4σ *ROSAT* source list on the same fields. The typical 1σ positional error in the *ROSAT* positions is 10 arcsec. The cross-correlation yielded a strong signal between the positions of detected *ASCA* sources and *ROSAT* 4σ source list (see Table 2 in Paper I). At angular separations less than 90 arcsec we found 26 matches between the *ASCA* and *ROSAT* source positions, compared to 8.5 expected on average. Three *ASCA* sources had more than one *ROSAT* counterpart within 90 arcsec and only three *ASCA* sources had no corresponding *ROSAT* counterpart.

Although there will be a number of chance coincidences amongst these matches, the *ASCA–ROSAT* positional cross-correlation does yield a much more accurate position for the vast majority of the *ASCA* sources. Moreover, statistical account can be made for the number of chance coincidences from the cross-correlation analysis (see below).

2.2 Optical

In Paper I, we were able to present a preliminary spectroscopic identification of the optical counterparts to the *ASCA* sources, based on those already identified as counterparts to the corresponding deep *ROSAT* sources in the cross-correlation. However, the optical identification of the 4σ list in the deep *ROSAT* survey was not complete, and this led to significant incompleteness in the optical identification ($\sim$ 50 per cent) for the *ASCA* source list.

In order to improve the completeness of the optical identifications for the *ASCA* source list, we carried out spectroscopic observations of optical counterparts to *ASCA*/*ROSAT* sources using the Low Dispersion Survey Spectrograph (LDSS) at the Anglo-Australian Telescope (AAT) on the nights of 1996 November 8–10. We operated LDSS using a mask comprising of a single 'long-slit' (1.7 arcsec wide) centred at 5500Å, with the high dispersion grism giving an overall instrumentation resolution of 13Å over the wavelength range $3800 < \lambda < 7800$. Throughout the run the conditions were less than ideal, with seeing ranging from 1.5 arcsec to over 3 arcsec; but all identifications reported here were obtained in less than 2.5 arcsec seeing. Little or no photometric time was obtained, and observations were only possible on the equivalent of 1.5 nights out of the 3 allocated. With LDSS, the slit mask and grism can be removed to give direct imaging, and we also obtained direct (unfiltered) images for most of the optical counterparts we observed. In most cases, the LDSS slit was oriented so that 2 or more optical counterparts could be positioned along the slit.

Optical counterparts for observation with LDSS were selected from APM scans of the UK Schmidt telescope (UKST) J survey plates and AAT J plates in each of the 2 *ASCA* areas (GSGP4 and QSF3) observable during the observing run. Candidates were simply selected on the basis on their proximity from the centroid of the *ROSAT* source which was the counterpart to the *ASCA* source. Orientation of the LDSS slit-mask allowed us to observe two or more optical counterparts for each integration. For each X-ray source, we continued to obtain spectra for optical counterparts until a plausible identification (e.g. QSO, cluster, emission-line object) was obtained.

Based on these observations, the revised identification list for the *ASCA* sources is presented in Table 1. *ASCA* sources with spectroscopic identifications from the LDSS observations are indicated with an asterisk. LDSS spectra for these objects are presented in Fig. 1. Since the slit was not positioned at the parallactic angle, and the seeing disk was typically much wider than the slit width, we chose not to flux the LDSS spectra, and they are presented here simply with counts on the ordinate. AUTOFIB spectra for the remainder of the sources (identified as part of the *ROSAT* deep survey) are published in Almaini (1996), or Shanks et al. (in preparation). Notes for some of the identifications are given at the foot of Table 1.

Following the LDSS observations, we now have an optical identification for up to 22 of the 26 *ASCA* sources, a completeness rate of 85 per cent. The breakdown of these initial classifications is summarised in Table 2. Of these 22 sources, there are 13 QSOs, 6 objects with narrow emission lines, 1 cluster, 1 star and 1 absorption-line galaxy. All but 2 of these sources, AXJ0057.6−2731 (a narrow-emission line galaxy) and AXJ1047.2−0028 (an absorption line galaxy) were found within 20 arcsec of the *ROSAT* X-ray position. At our optical detection limit on the UKST photographic plates ($B \sim 23$), the space density of QSOs is $\sim 200\,{\rm deg}^{-2}$ (Schade et al. 1996). Thus we would expect 0.02 QSOs within 20 arcsec of each X-ray source position by chance, corresponding to only 0.5 QSOs over the entire survey.

It is difficult to make a definitive identification of the nature of the six narrow-emission-line galaxies identified in this survey. In the four cases where it is possible to make a reliable measurement of the [OIII]λ5007/Hβ ratio, all but one (the counterpart to AXJ0057.6–2731) have emission-line ratios [OIII]λ5007/H$\beta > 3$. Based on the standard Baldwin, Phillips and Terlevich (1981) line-ratio diagnostic, this observation in itself is insufficient to classify these objects unambiguously as starburst galaxies or Seyfert 2 galaxies. Other line ratios, most notably [NII]/Hα, are also required. However, in the detailed study of narrow-emission line galaxies identified as counterparts to *ROSAT* X-ray sources by Boyle et al. (1995), the vast majority (7/8) of the narrow-emission line galaxies with [OIII]λ5007/H$\beta > 3$, also have [NII]/Hα emission line ratios which identify them as Seyfert 2 galaxies rather than starburst galaxies (see Fig 3. in Boyle et al. 1995). The 2-10 keV X-ray luminosities of the narrow-emission-line galaxies identified in this survey ($> 10^{42.5}\,{\rm erg\,s^{-1}}$) are also inconsistent with starburst galaxies. We tentatively conclude, therefore, that the ma-

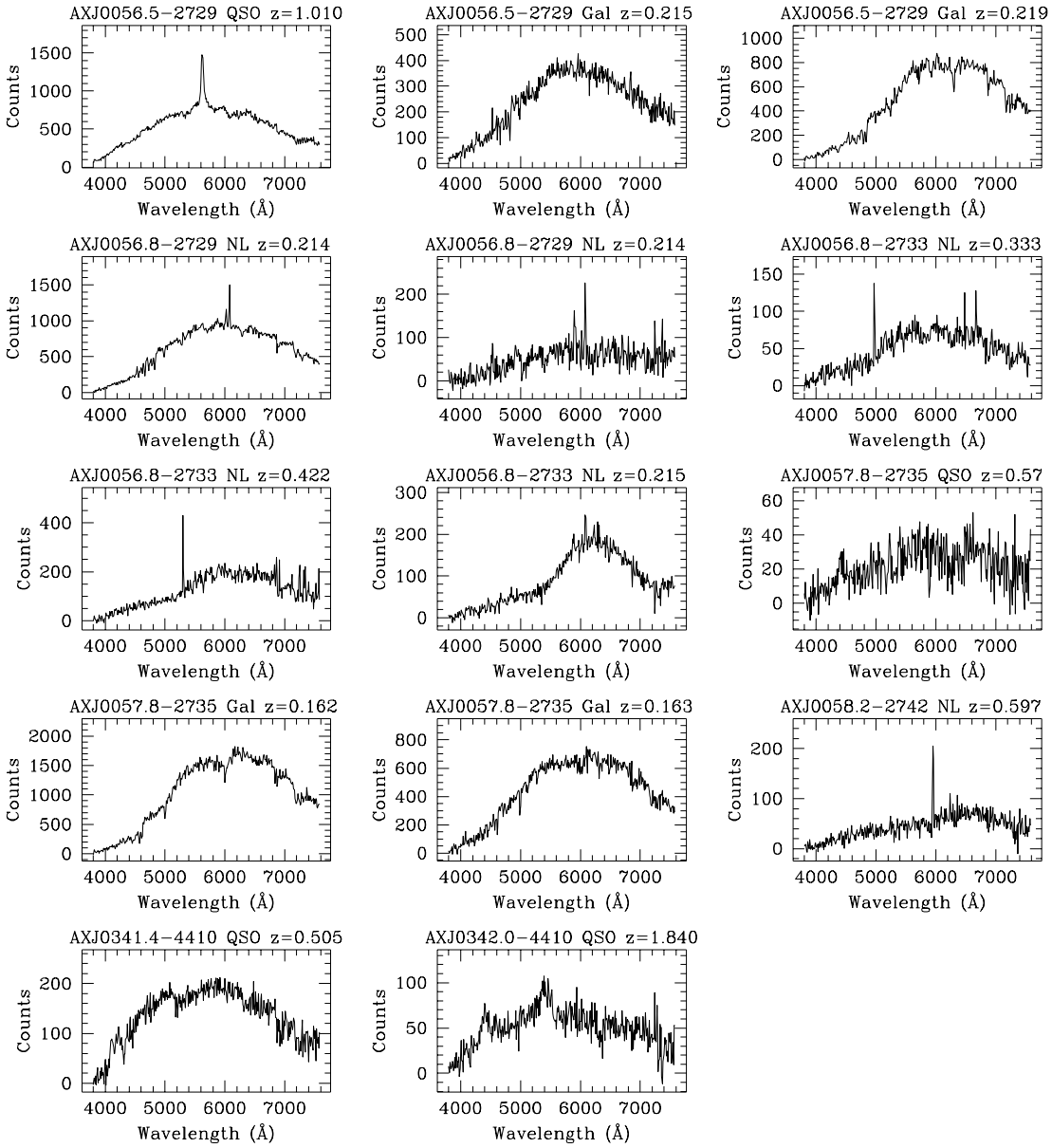

Figure 1. LDSS spectra of the optical counterparts to the *ASCA* sources.

jority of narrow-emission-line objects identified in this survey are more likely to be Seyfert-2 galaxies (Type 2 AGN) than starburst galaxies. However, further observations will be required to determine their nature unequivocally.

Tresse et al. (1996) estimate that approximately 17 per cent of field galaxies with $I < 22.5$ have emission line ratios consistent with active galaxies (Seyfert 2 or Liners). Based on the galaxy number-magnitude counts of Metcalfe et al. (1991), this corresponds to a surface density of 800 active galaxies per square degree at $B < 23$, implying that a total of ~ 2 such objects would be found by chance amongst the optical counterparts found within 20 arcsec of the *ROSAT* source positions associated with *ASCA* detections. In total, seven narrow-emission-line galaxies were identified at these separations, including a narrow-emission-line galaxy found only 8 arcsec from an *ASCA* source position with no *ROSAT* counterpart. Of these seven sources, five have been tentatively identified as the counterpart to an *ASCA* source, the remaining two are the more distant optical counterparts to *ASCA* sources with an alternative identification (AXJ0056.8−2733 and AXJ1046.1−0020). This confusion rate is therefore broadly consistent with that predicted from the observations of Tresse et al. (1996).

There is one narrow-emission-line galaxy (AXJ0057.6–2731) identified as a counterpart to an *ASCA* source which was not found within 20 arcsec of the corresponding *ROSAT* source position. It is probable that this identification (a late-type galaxy with weak [OII] and [OIII] emission) is not the correct counterpart to the *ASCA* source. This galaxy is 34 arcsec and 95 arcsec distant from the *ROSAT* and *ASCA* source positions respectively and the separation between *ROSAT* and *ASCA* positions is also large (> 60 arcsec).

Table 1. *ASCA* Survey Catalogue

Name	*ASCA* position RA (2000) Dec h m s ° ′ ″	Optical Position RA (2000) Dec h m s ° ′ ″	Offset *ASCA* (″)	Offset *ROSAT* (″)	Count rate 2-10keV (10^{-3} ct s^{-1})	B (mag)	Spectroscopic ID
AX J0056.4-2748	00 56 25.6 −27 48 48	00 56 23.6 −27 48 56	27	6	5.07±1.24	16.0	**QSO z=0.145**
AX J0056.5-2729	00 56 31.1 −27 29 47	00 56 34.0 −27 29 52	39	17	3.30±1.14	16.9	**QSO z=1.010**[*,1]
		00 56 34.0 −27 29 52	39	17	3.30±1.14	16.9	Galaxy z=0.215[*,1]
		00 56 32.6 −27 29 59	23	22	3.30±1.14	19.3	Galaxy z=0.219[*,1]
AX J0056.8-2729¶	00 56 49.9 −27 29 28	00 56 50.3 −27 29 34	8		1.90±0.88	23.0	**NL z=0.214**[*,2]
		00 56 51.7 −27 28 57	39		1.90±0.88	18.1	NL z=0.214[*,2]
AX J0056.8-2733	00 56 51.0 −27 33 09	00 56 50.0 −27 33 21	18	5	1.66±0.60	22.7	**NL z=0.333**[*,3]
		00 56 52.2 −27 33 39	34	31	1.66±0.60	21.6	NL z=0.422*
		00 56 48.8 −27 33 31	37	16	1.66±0.60	21.9	NL z=0.215*
AX J0057.0-2741	00 56 59.4 −27 41 00	00 56 56.9 −27 40 30	45	8	1.06±0.46	21.9	**Cluster z=0.561**[4]
AX J0057.0-2741‡		00 57 04.4 −27 40 22	76	15	1.06±0.46	21.6	Continuum
AX J0057.3-2731	00 57 20.8 −27 31 53	00 57 24.4 −27 32 01	49	8	3.07±0.36	19.5	**QSO z=1.209**
AX J0057.6-2731†	00 57 38.5 −27 31 13	00 57 45.6 −27 31 17	96	37	1.13±0.44	20.1	**NL z=0.316**[5]
AX J0057.8-2735	00 57 48.4 −27 35 56	00 57 46.8 −27 35 37	28	3	0.87±0.37	22.5	**QSO z=0.57**[*,6]
		00 57 48.0 −27 35 54	6	27	0.87±0.37	18.9	Galaxy z=0.162[*,6]
		00 57 49.4 −27 36 22	29	60	0.87±0.37	18.0	Galaxy z=0.163[*,6]
AX J0058.2-2742	00 58 11.9 −27 42 44	00 58 13.5 −27 42 11	39	16	1.70±0.64	22.2	**NL z=0.597***
AX J0341.1-4412	03 41 04.5 −44 12 04	03 41 04.2 −44 12 06	4	8	1.19±0.36	21.6	**QSO z=1.808**
AX J0341.4-4410	03 41 23.0 −44 10 47	03 41 19.3 −44 10 30	43	7	1.01±0.29	21.5	**QSO z=0.505***
AX J0341.8-4414¶	03 41 45.6 −44 14 07				1.00±0.31		**No reliable c'part**
AX J0341.8-4402	03 41 47.1 −44 02 24	03 41 44.3 −44 02 49	39	14	0.92±0.31	21.7	**QSO?**[7]
AX J0341.8-4353	03 41 51.2 −43 53 48	03 41 52.2 −43 53 26	24	7	3.00±0.54	12.0	**G star**
AX J0342.0-4410†	03 42 01.1 −44 10 53	03 42 05.6 −44 09 43	85	7	1.26±0.28	21.1	**QSO z=1.840**[*,8]
AX J0342.0-4403	03 42 02.4 −44 03 51	03 42 03.7 −44 03 45	15	3	0.99±0.30	19.2	**QSO z=0.635**
AX J0342.3-4412	03 42 19.1 −44 12 38	03 42 18.4 −44 12 50	14	5	0.82±0.31	21.8	**QSO z=1.091**
AX J0342.3-4412‡		03 42 16.7 −44 11 54	52	2	0.82±0.31	21.7	Not observed
AX J0342.5-4409†	03 42 32.4 −44 09 35	03 42 24.1 −44 09 44	90	11	0.92±0.37	22.1	**Not observed**
		03 42 24.6 −44 09 50	85	14	0.92±0.37	20.6	Not observed
AX J0342.6-4404	03 42 35.4 −44 04 41	03 42 38.5 −44 04 50	34	1	1.39±0.42	20.4	**QSO z=0.377**
AX J1046.1-0020	10 46 05.1 −00 20 48	10 46 05.9 −00 20 25	26	12	1.54±0.42	20.6	**QSO z=1.070**
AX J1046.1-0020‡		10 46 05.2 −00 22 02	74	14	1.54±0.42	20.6	NL z=0.295
AX J1046.2-0022	10 46 13.4 −00 22 16	10 46 15.0 −00 22 48	40	13	1.26±0.30	20.8	**QSO z=1.952**
AX J1046.4-0021†	10 46 26.6 −00 21 09	10 46 33.6 −00 21 40	109	20	1.14±0.34	18.5	**NL z=0.130**
AX J1046.7-0021¶	10 46 39.8 −00 21 40				0.97±0.37		**No reliable c'part**
AX J1046.9-0026†	10 46 54.4 −00 26 42	10 46 53.4 −00 25 44	60	4	1.84±0.60	21.3	**NL z=0.435**
AX J1047.1-0025†	10 47 09.3 −00 25 39	10 47 12.3 −00 26 18	60	19	2.65±0.30	22.1	**Low S/N**
AX J1047.2-0028	10 47 12.4 −00 28 00	10 47 14.8 −00 28 29	46	27	4.17±1.27	18.2	**Galaxy z=0.080**

Notes

Entries in bold refer to the optical identification adopted in initial sample.

* Observed with LDSS

† Association with identified *ROSAT* counterpart ignored in the revised sample.

‡ Alternative *ROSAT* identification associated with *ASCA* source. Optical counterpart ignored in the revised sample.

¶ No *ROSAT* counterpart within 90arcsec.

1. A QSO and a $z \sim 0.215$ galaxy cluster are both detected as counterparts to the same *ASCA* source.

2. Two galaxies observed at the same redshift. They may comprise a possible cluster, but no obvious cluster is seen in the direct image. Both galaxies have emission-line ratios consistent with Seyfert 2 galaxies (see text).

3. There are several narrow-emission-line galaxies identified within the *ASCA* error box. However, the $z = 0.333$ object closest to the corresponding *ROSAT* centroid is most likely to be the correct identification. Its emission-line ratios are consistent with a Seyfert 2 galaxy.

4. Cluster identification from Couch et al. (1985).

5. The *ROSAT* and *ASCA* source positions are widely separated. The $z = 0.316$ narrow-emission line galaxy was originally identified as a counterpart to the *ROSAT* source, but it exhibits a large separation from both the *ROSAT* and *ASCA* centroids. The source is coincident with the outer regions of one of the spiral arms of the brightest galaxy $B = 13$ in the GSGP4 field (GSA002, see Peterson et al. 1986. However, the *ASCA* source is unlikely to be associated with the galaxy ($z = 0.019$) given the implied X-ray-to-optical flux ratio for a galactic source at this redshift.

6. The closest object to the *ROSAT* centroid is a probable $z = 0.57$ QSO observed at low signal-to-noise. The closest object to *ASCA* centroid is a $z = 0.162$ galaxy, with an additional galaxy at the same redshift some 20 arcsec further away from the *ROSAT* position.

7. Radio source: $S_{20\mathrm{cm}}$=298mJy

8. Radio source: $S_{20\mathrm{cm}}$=189mJy

Table 2. Identification summary for the *ASCA* survey

Classification	Number	
	Initial	Revised
QSO	13	10
Narrow-emission line objects	6	1
Cluster	1	4
Star	1	1
Absorption-line galaxy	1	1
No identification	4	9

It is therefore one of the positional coincidences between the *ASCA* and *ROSAT* catalogues most likely to have been chance and its identification was one of those removed from the revised catalogue (see below).

There may be other optical identifications that are also ambiguous. We have included in the list of QSOs at least 2 sources whose classification is uncertain. One *ASCA* source, AXJ0341.8–4402 has been associated with a faint ($B = 21.7$) blue stellar object 14 arcsec distant from the *ROSAT* position and 39 arcsec from the *ASCA* centroid. We were frustrated in our attempts to obtain a spectrum for this object by the weather conditions. From observations made with the Australia Telescope (Boyle et al. 1993) this object is also a relatively strong radio-source ($S_{20\rm cm} = 298\,\mu$Jy). Thus the most likely identification for this source is a QSO, although it will require further confirmation. The closest optical counterpart to the *ROSAT* source coincident with AXJ0057.8–2735 is identified as a $z = 0.57$ QSO based on a low signal-to-noise spectrum containing one emission line. It is possible that the correct optical counterpart to the *ASCA* source is one of the pair of $z = 0.162$ galaxies, one of which is only 6 arcsec from the *ASCA* centroid. However, both these galaxies are > 25 arcsec from the *ROSAT* position and both are unlikely to be the correct identification if the *ROSAT* and *ASCA* detections correspond to the same source. Finally, the QSO identified as the counterpart to AXJ0056.5–2729 is a rather remarkable object. Originally identified as a cluster in Paper I, the LDSS observations revealed a $z = 1.01$ QSO lying behind the cluster at $z = 0.217$. It is possible that both the cluster and the QSO contribute to the X-ray emission.

Some of the *ASCA* sources initially associated with narrow-emission-line galaxies may also have been incorrectly identified. For example, although the *ASCA* source AXJ0056.8–2729 has been identified as a $z = 0.214$ narrow-emission-line galaxy located only 8 arcsec from the *ASCA* centroid, a narrow-emission-line galaxy with an identical redshift was also observed 39 arcsec from the *ASCA* source. The X-ray emission may therefore originate from a cluster or group which comprises these two galaxies (possibly the outer regions of the $z = 0.215$ cluster associated with AXJ0056.5–2729 some 3–4 arcmins distant). However, no strong concentration of galaxies in visible on the LDSS direct image of this field.

As described above, there is a probability that at least some of the *ROSAT*/*ASCA* correlations have come about through chance coincidences. The *ROSAT*/*ASCA* coincidences listed in table 1 are based on separations up to 90 arcsecs. At this separation, there are 26 observed coincidences between *ROSAT* and *ASCA* sources (3 *ASCA* sources have two *ROSAT* counterparts at this separation and 3 *ASCA* sources have no *ROSAT* counterpart), of which ~ 9 will be random coincidence (see Paper I).

In order to account for this in the analysis below, we can remove from the identification list the counterparts to the 9 *ROSAT* sources sources with the largest *ASCA*-*ROSAT* separation. This results in the rejection of the additional *ROSAT* counterparts to *ASCA* sources AXJ0057.0–2741, AXJ0342.3–4412 and AXJ1046.1–0020. It also removes the spectroscopically identified counterparts to AXJ0057.6-2731 (a $z = 0.316$ narrow-emission-line galaxy), AXJ0342.0–4410 ($z = 1.840$ QSO), AXJ0342.5–4409 (not observed) AXJ1046.4–0021 ($z = 0.130$ narrow-emission-line galaxy), AXJ1046.9–0026 ($z = 0.43$ narrow-emission-line galaxy) and AXJ1047.1–0025 (an object with a low signal-to-noise ratio spectrum). This leaves no *ASCA*-*ROSAT* coincidences with separations larger than 1 arcmin. If we further assume that the X-ray sources AXJ0057.8–2735 and AXJ0056.5-2729 classified as clusters rather than QSOs and that AXJ0056.8–2729 should be classified as a cluster rather than a narrow-emission-line galaxy, then the revised composition of the *ASCA* sources is 10 QSOs, 1 narrow-emission-line galaxy, 4 clusters, 1 star and 1 galaxy. In this case there are no reliable identifications for a further 9 objects; a completeness rate of 65 per cent.

The composition of the *ASCA* source list for the initial and revised identification lists is summarised in table 2. It is likely that the true composition of the *ASCA* source list will lie somewhere between these two extremes. Although we were 'optimistic' in assigning identifications to some chance *ROSAT*/*ASCA* positional coincidences in our initial sample, we were 'pessimistic' (particularly with regard to emission-line objects) in our identification rates in the revised list. In the analysis that follows, we will use both the initial and revised lists to determine the likely systematic errors in any estimation of the properties of the AGN population that forms the bulk of the *ASCA* sample, whichever list is chosen.

3 ANALYSIS

For the purposes of the following analysis, we have combined the emission-line objects identified in our *ASCA* source list (QSOs and narrow-emission-line galaxies) with the bright sample of AGN identified by Grossan (1992) from the Large Area Sky Survey/Modulation Collimator (LASS/MC) catalogue (Remillard et al. 1986) obtained from *HEAO 1* mission (Wood et al. 1984). The LASS/MC AGN (LMA) sample comprises 96 predominantly low redshift ($z < 0.2$) AGN (85 Seyfert 1 and 11 Seyfert 2 galaxies), selected at bright flux limits ($S_{2-10} > 2{\times}10^{-11}\,\rm erg\,cm^{-2}\,s^{-1}$) and is 90 per cent complete at galactic latitudes $b > 20^{\circ}$. This sample has also previously been used by Ceballos and Barcons (1996) to derive the $z < 0.2$ AGN luminosity function in the 2-10 keV band. Combining these two samples gives us a wide range in luminosity and redshift over which to determine the evolution of the AGN luminosity function (LF).

We carried out the analysis for two AGN samples: Type 1 AGN and Type 1 + Type 2 AGN. The Type 1 AGN sample comprises the QSOs identified in the *ASCA* survey and the Seyfert 1 galaxies in the Grossan (1992) sample. The

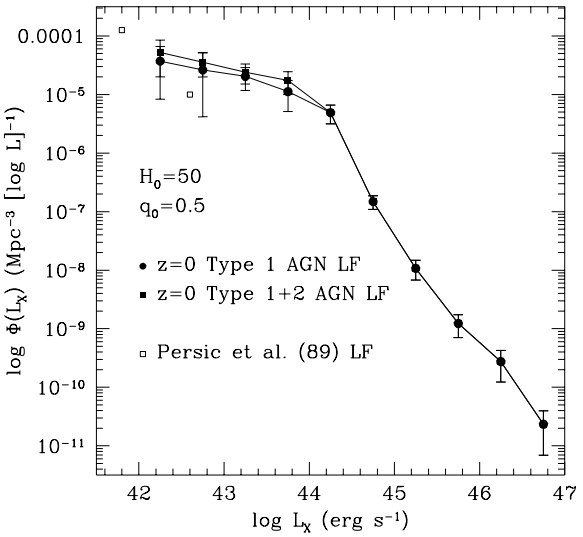

Figure 2. $1/V_a$ estimate for the 2-10 keV luminosity function for Type 1 and Type 1+2 AGN.

Type 1 + Type 2 AGN sample also includes the narrow-emission-line galaxies identified in the *ASCA* sample (tentatively identified as Seyfert 2-like objects) and the bona-fide Seyfert 2 galaxies in Grossan (1992). Unfortunately, there are too few Type 2 AGN to carry out a meaningful analysis of the LF for this sample alone. For ease of reference the samples will be referred to as the Type 1 AGN and Type 1 + Type 2 AGN in the analysis below. However, we note there is still uncertainty over the identification of the six narrow-emission-line galaxies in the *ASCA* sample as Seyfert 2 galaxies.

We first carried out a standard $\langle\frac{V_e}{V_a}\rangle$ analysis (Avni and Bahcall 1980) of the combined LMA plus *ASCA* samples. For consistency with previous analyses, the 'canonical' value of $\alpha_X = 0.7$ (Mushotzky 1982) was adopted for the AGN energy spectral index in the 2-10 keV band. This is marginally softer than, but not inconsistent with, the mean AGN 2-10 keV spectral index measured in our sample $\alpha_X \sim 0.5\pm0.2$ (see Georgantopoulos et al. 1997, in preparation, hereinafter Paper III). The adoption of $\alpha_X = 0.7$ makes little or no difference to the computed $\langle\frac{V_e}{V_a}\rangle$; $\alpha_X = 0$ and $\alpha_X = 1.0$ change it by no more than ±0.01. Similarly, any change in α_X results in the identical change in the derived exponent of power-law luminosity evolution (k, see below) and estimates of the AGN contribution to the X-ray background are independent of α_X.

The $\langle\frac{V_e}{V_a}\rangle$ results are reported in Table 3, where the error on $\langle\frac{V_e}{V_a}\rangle$ is estimated from $1/\sqrt{12N}$. All entries in Table 3 are at least 4σ higher than the 'no-evolution' $\langle\frac{V_e}{V_a}\rangle = 0.5$ value all samples. There is no significant difference between any of the $\langle\frac{V_e}{V_a}\rangle$ values listed in this table, whether they were derived for the Type 1 or Type 1 + Type 2 AGN samples or with the inclusion of the initial or revised *ASCA* samples. These values for $\langle\frac{V_e}{V_a}\rangle$ are consistent with that already derived for the AGN in the LMA sample by Grossan (1992); $\langle\frac{V_e}{V_a}\rangle = 0.63$. Grossan (1992) was concerned that this high value of $\langle\frac{V_e}{V_a}\rangle$ might be due to systematic errors in the LMA sample, (as opposed to evolution), but was unable to identify a potential source of error which could give rise to this high value of $\langle\frac{V_e}{V_a}\rangle$. However, we have also obtained similar values of $\langle\frac{V_e}{V_a}\rangle$ (albeit with larger errors) when we combined either the initial or revised *ASCA* sample with the more limited sample of 26 AGN in Piccinotti et al. (1982); $0.61 \pm 0.05 < \langle\frac{V_e}{V_a}\rangle < 0.65 \pm 0.04$ or when we analysed the *ASCA* sample on its own $0.59 \pm 0.09 < \langle\frac{V_e}{V_a}\rangle < 0.65 \pm 0.08$. We therefore conclude that there is significant evidence for AGN evolution in the 2-10 keV band.

Table 3. $\langle\frac{V_e}{V_a}\rangle$ values derived for AGN in the *ASCA* and LMA samples.

AGN	Initial		Revised	
	N	$\langle\frac{V_e}{V_a}\rangle$	N	$\langle\frac{V_e}{V_a}\rangle$
Type 1 + Type 2	115	0.63 ± 0.03	108	0.62 ± 0.03
Type 1	98	0.64 ± 0.03	95	0.62 ± 0.03

We then carried out a maximum likelihood analysis to derive the best-fit parameters of a number of models used to describe the 2-10 keV luminosity function and its cosmological evolution with redshift.

We chose a two-power-law representation for the QSO LF, identical to the model used to fit successfully the 0.5-2 keV QSO LF by Boyle et al. (1994):

$$\Phi(L_X) = K_1 L_X^{-\gamma_1} \qquad L_X < L_X^*(z=0)$$

$$\Phi(L_X) = K_2 L_X^{-\gamma_2} \qquad L_X > L_X^*(z=0)$$

This model has already been shown to provide a good fit to the 2-10 keV AGN LF by Ceballos and Barcons (1996). Moreover, Grossan (1992) has already shown that a single-power-law is not an acceptable fit to this LF.
A standard power-law luminosity evolution model was used to parameterise the cosmological evolution of this luminosity function:

$$L_X^*(z) = L_X^*(0)(1+z)^k$$

In order to derive the 'best-fit' values and errors for the 4 free parameters in this model, γ_1, γ_2, k and L^*, we used our standard likelihood minimisation procedure (Boyle et al. 1988). K_1 [$= K_2(L_X^*/10^{44}\mathrm{erg\,s^{-1}})^{(\gamma_1-\gamma_2)}$] is obtained from the normalisation of the luminosity function to the total number of objects identified in the combined sample.

As before, the acceptability of the model was derived from the 2D Kolmogorov-Smirnov statistic applied to the joint distribution in luminosity and redshift.

The model was tested against the combined LMA plus initial and revised *ASCA* samples, and the model was run for both the Type 1 and Type 1 + Type 2 AGN samples. The results are reported in Table 4. The rate of the cosmological evolution derived from these fits was also used to generate the binned $1/V_a$ estimate of the de-evolved LF for both Type 1 and Type 1 + Type 2 AGN in the initial sample which is plotted in Fig 2. The error bars on this figure are based on Poisson statistics. The binned estimates of the

Table 4. The 2-10 keV AGN LF parameters

Sample	AGN	N	γ_1	γ_2	$\log L^*$	k	Φ^* $\mathrm{Mpc}^{-3}[10^{44}\,\mathrm{erg\,s}^{-1}]^{-1}$	P_{KS}
LMA + ASCA initial	Type 1 + Type 2	115	1.91	2.98	44.13	2.04	9.52×10^{-7}	0.20
LMA + ASCA revised	Type 1 + Type 2	108	1.89	2.97	44.14	2.03	9.19×10^{-7}	0.22
LMA + ASCA initial	Type 1	98	1.73	2.96	44.15	2.01	8.24×10^{-7}	0.27
LMA + ASCA revised	Type 1	95	1.73	2.96	44.16	2.00	8.21×10^{-7}	0.25
68% confidence regions			$^{+0.14}_{-0.20}$	$^{+0.06}_{-0.08}$	$^{+0.10}_{-0.10}$	$^{+0.16}_{-0.22}$		
95% confidence regions			$^{+0.20}_{-0.70}$	$^{+0.18}_{-0.25}$	$^{+0.34}_{-0.61}$	$^{+0.34}_{-0.46}$		

2-10 keV LF from Persic et al. (1989) are also plotted on this figure. The Persic et al. (1989) LF is based on *HEAO 1* A-2 observations of the complete sample of Seyferts in the CfA optically-selected sample and provides an independent estimate of the 2-10 keV LF at low luminosities. We have plotted the lower estimates of the LF from Persic et al. (1989). The Persic et al. (1989) LF exhibits good agreement with the faint end of the LF derived in this analysis.

We can see from Table 4 that a two-power-law LF with power-law luminosity evolution produces a good fit to the data. There is no significant difference between the model fits to the initial and revised *ASCA* data-sets. The main difference between the model fits to the Type 1 and Type 1 + Type 2 AGN samples is in the slope of the faint end of the 2-10 keV LF. As borne out by Fig. 2, the addition of Type 2 AGN into the fit marginally steepens the faint end of the LF.

The values for parameters of the $z = 0$ LF obtained here are different at the 95 per cent confidence level to those derived by Ceballos and Barcons (1996); $\gamma_1 = 2.11$, $\gamma_2 = 3.27$, and $\log L^* = 44.51$. Ceballos and Barcons (1996) computed the LF from the $z < 0.2$ AGN in the LMA sample using the evolution derived by Maccacaro et al. (1991) for the EMSS sample in the 0.3-3.5 keV band to 'de-evolve' the LF back to $z = 0$. The EMSS evolution is stronger, $L \propto (1+z)^{2.6}$, than that derived here, which may, in part, account for some of the discrepancy seen.

Although the 95 per cent confidence regions on the LF parameter values (γ_1, γ_2, L^*) quoted in Table 4 are relatively large, they are highly correlated. A decrease in the value of γ_1 leads to decrease in the derived value of L^* and corresponding increase in γ_2. The error on k is largely uncorrelated with any of the LF parameters, and remains the major uncertainty in the determination of the AGN contribution to the 2-10 keV X-ray background (see below).

4 DISCUSSION

The predicted 2-10 keV AGN number-flux relation, $\log N - \log S$, for the two-power-law LF model is plotted in Fig. 3 for both Type 1 and Type 1 + Type 2 AGN. These predicted $\log N - \log S$ relations were based on an extrapolation the LFs to $L = 10^{39}\,\mathrm{erg\,s}^{-1}$ and $z = 4$ (see below). We also show the observed QSO + narrow-emission-line galaxy $\log N - \log S$ from the *ASCA* survey for the initial sample (corrected for incompleteness). No error bars have been included on these points, because they are not independent.

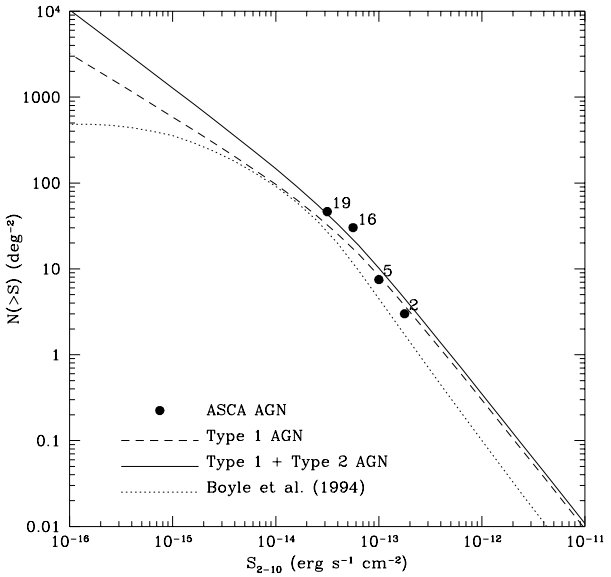

Figure 3. The predicted $\log N - \log S$ relations for Type 1 AGN and Type 1 + Type 2 AGN based on the evolutionary models described in the text. The surface density of QSOs and narrow-emission-line galaxies identified in the initial *ASCA* sample are indicated by the filled dots. The predicted 2-10 keV QSO $\log N - \log S$ based on model H in Boyle et al. (1994) and extrapolated with $\alpha_X = 1$ is shown as a dotted line.

However the numbers next to each point represent the number of objects comprising each estimate of the surface density. The models accurately predict the correct observed numbers in the *ASCA* survey, although the *ASCA* survey was of course used, in part, to determine the parameters of the LF. The observed and predicted number-redshift relation, n(z), for Type 1 + Type 2 AGN in the *ASCA* survey are also plotted in Fig. 4. Although the numbers are small, the model fit is not inconsistent with the data.

We have also used the LF parameters to estimate the contribution of Type 1 and Type 1 + Type 2 AGN to the total 2-10 keV XRB. We used the 2-10 keV XRB, $I = 19.5 \times 10^{-12}\,\mathrm{erg\,cm}^{-2}\,\mathrm{s}^{-1}\,\mathrm{deg}^{-2}$ observed by Chen, Fabian & Gendreau (1996). Since the faint end of the LF is steep, the total contribution of AGN to the XRB is highly dependant on the faintest X-ray luminosities to which the LF is extrapolated. To a lesser extent, the total contribution is also dependent on the redshift to which the evolution of

Table 5. Predicted AGN contribution, $f_{\rm XRB}$, to the 2-10 keV X-ray background

Limits of integration	LF model	$f_{\rm XRB}$ (per cent) Type 1	Type 1 + 2
$L > 10^{42}\,{\rm erg\,s^{-1}}$, $z < 2$	Best-fit	27	39
$L > 10^{42}\,{\rm erg\,s^{-1}}$, $z < 4$	Best-fit	33	48
$L > 10^{41}\,{\rm erg\,s^{-1}}$, $z < 4$	Best-fit	37	61
$L > 10^{40}\,{\rm erg\,s^{-1}}$, $z < 4$	Best-fit	39	72
$L > 10^{39}\,{\rm erg\,s^{-1}}$, $z < 4$	Best-fit	41	80
$L > 10^{39}\,{\rm erg\,s^{-1}}$, $z < 4$	$\gamma_1 + 1\sigma$	59	> 100
$L > 10^{39}\,{\rm erg\,s^{-1}}$, $z < 4$	$k + 1\sigma$	46	93

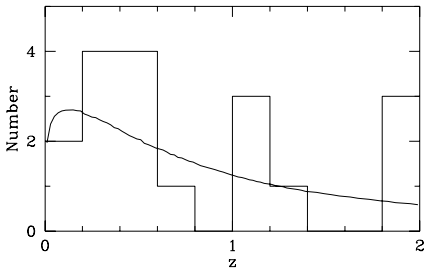

Figure 4. The observed and predicted n(z) relation for Type 1 + Type 2 AGN in the initial *ASCA* sample.

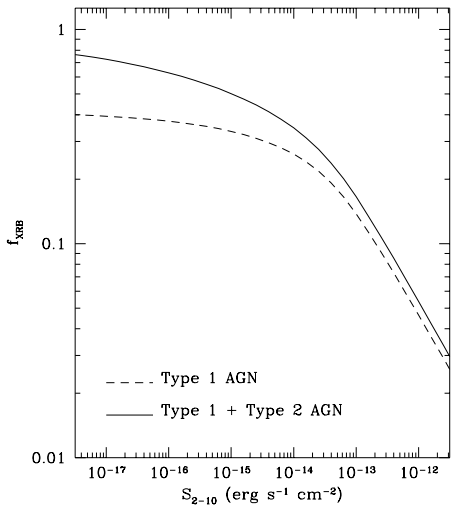

Figure 5. The predicted contribution of Type 1 + Type 2 AGN to the 2-10 keV X-ray background, $f_{\rm XRB}$.

the LF extrapolated. In Table 5 we list the predicted contributions from AGN based on the extrapolations of the Type 1 and Type 1 + Type 2 LFs derived above. If we integrate the LF down to $10^{42}\,{\rm erg\,s^{-1}}$ and to $z < 2$, the faintest luminosities and the highest redshifts sampled in the LASS/MC and *ASCA* samples, we obtain a total contribution to the $2-10$ keV XRB of 27 per cent for Type 1 AGN and 39 per cent for Type 1 + Type 2 AGN. In contrast, by extending the integration of the LF to $10^{39}\,{\rm erg\,s^{-1}}$ (the upper limits on the faintest AGN luminosities in the Persic et al. sample), and increasing the redshift limit to $z = 4$ (with no evolution of the LF at $z > 2$, see Boyle et al. 1994) we derive total contributions of 41 per cent for Type 1 AGN and 80 per cent for Type 1 + Type 2 AGN. When the LF is extrapolated down to these low luminosities, the error on the slope of the faint end of the LF dominates the statistical uncertainty in the estaimate AGN contribution to the XRB. Increasing the slope of the faint end of the LF by its 1σ error yields a total contribution of almost 60 per cent for Type 1 AGN and over 100 per cent for Type 1 + Type 2 AGN, saturation occuring at $S_{2-10} \sim 2.5 \times 10^{-17}\,{\rm erg\,cm^{-2}\,s^{-1}}$. The only other parameter whose statistical uncertainty significantly affects the AGN contribution to the XRB is the evolution parameter. The 1σ upper limit for k yields total contributions of 46 per cent and 93 per cent for Type 1 and Type 1 + Type 2 AGN respectively.

Although upper limits for AGN in Persic et al. (1989) suggest AGN 2-10 keV luminosities as low as $10^{39}\,{\rm erg\,s^{-1}}$, we note that the local 2-10 keV luminosity density obtained by integrating the Type 1 + Type 2 $z = 0$ LF down to $10^{42}\,{\rm erg\,s^{-1}}$ is $4.87 \times 10^{38}\,{\rm erg\,s^{-1}Mpc^{-3}}$. This is close to the 95 per cent confidence upper limit of $4.77 \times 10^{38}\,{\rm erg\,s^{-1}Mpc^{-3}}$ obtained for the local Type 1 + Type 2 AGN 2-10 keV luminosity density by Barcons et al. (1995) from consideration of the *HEAO 1* A-2 all-sky maps and the *IRAS* 12 micron source catalogue. Decreasing the minimum luminosity to $10^{39}\,{\rm erg\,s^{-1}}$ in the calculation of the local 2-10 keV luminosity density yields a value $8.10 \times 10^{38}\,{\rm erg\,s^{-1}Mpc^{-3}}$ which is high compared to the Barcons et al. (1995) upper limit.

If the AGN LF does cut-off at $L < 10^{42}\,{\rm erg\,s^{-1}}$, then we are forced to conclude that there is a significant residual contribution to the 2-10 keV XRB from sources which we have yet to identify. These could be heavily absorbed AGN (e.g. Madau et al. 1994, Comastri et al. 1995) or precursor AGN at high redshift (Boldt and Leiter 1993).

In constrast, if the AGN LF can be extended to significantly fainter luminosities then AGN could supply most of the 2-10 keV background. In this case, there is still the outstanding issue of matching the observed AGN spectrum to that of the X-ray background. Although the mean 2-10 keV spectral index for AGN in this analysis ($\alpha_X = 0.5 \pm 0.25$) is consistent with the observed value for the X-ray background at these energies, it is also equally consistent with the 'canonical' value for low redshift range AGN $\alpha_X = 0.7$ (Mushotsky 1982). The AGN in this analysis could, in principle, readily exhibit a harder spectrum than $\alpha_X = 0.7$ if the instrinsic AGN spectral index hardened with energy. At the mean redshift of the sample ($z \sim 0.7$), the observed

ASCA energy range corresponds to 3.4-17 keV, significantly harder than the energy range sampled at $z = 0$. Evidence for the hardening of the X-ray spectral index with energy, possibly due to Compton reflection, has been found previously (Pounds et al. 1990, Nandra & Pounds, 1994) and has also been used to explain the observed spectrum of the XRB (Tucker & Schwarz 1986, Boyle 1996). However, as yet there is no strong evidence for any hardening of the X-ray spectral slope with energy in this sample and further data will be required before a more accurate picture of the spectral characteristics of these AGN can be built up.

In Fig. 3 we also show the predicted QSO $\log N - \log S$ based on the fit to the 0.3-3.5 keV XLF made by Boyle et al. (1994, model H) based on the *ROSAT* (0.5-2 keV) and Einstein (0.3-3.5 keV) surveys and extrapolated to the 2-10 keV band using $\alpha_X = 1$. To maintain consistency with the *ASCA* $\log N - \log S$, the 0.3-3.5 keV LF was extrapolated to $L_X = 10^{39}\,\mathrm{erg\,s^{-1}}$, and $z < 4$. The predicted *ROSAT* QSO $\log N - \log S$ based on the softer X-ray data lies a factor of two below the *ASCA* QSO/narrow-emission-line-galaxy $\log N - \log S$ at all fluxes, and suggests that the *ASCA* survey is detecting more AGN than *ROSAT* at an equivalent flux limit, assuming a straightforward extrapolation of the soft (0.5-2 keV) X-ray spectral slope $\alpha_X = 1$ (Wilkes and Elvis 1987). A harder spectral slope would give greater agreement between the *ASCA* and extrapolated *ROSAT* counts.

5 CONCLUSIONS

We have obtained spectroscopic identification for a sample of 26 *ASCA* sources detected in three deep *ROSAT* fields. The optical identification for the sample lies between 65 and 84 per cent. Most of the objects are identified as QSOs or narrow-emission-line galaxies, with between 10 and 13 QSOs and between 1 and 5 narrow-emission-line galaxies in the final sample. When we combine this sample with a larger, predominantly low redshift ($z < 0.2$) sample, we find significant evidence for cosmological evolution, with a luminosity evolution law $L_X \propto (1+z)^{2.04^{+0.16}_{-0.22}}$. Based on the derived evolution and the 2-10 keV luminosity function, the predicted contribution of QSOs to the 2-10 keV X-ray background is 40 ± 20 per cent. If the narrow-emission-line galaxies identified in this analysis are also included (tentatively identified as Seyfert 2 galaxies), then the total AGN contribution to the X-ray background could amount to 80 ± 20 per cent. However, uncertainties over the extent to which the $z = 0$ AGN LF can be extrapolated to low luminosities, could still leave room for an as yet unidentified class of source to comprise a significant component of the 2-10 keV XRB.

If AGN are to prove the dominant source of the X-ray background, then their average spectral properties must be consistent with that of the background. Currently, the results on the 2-10 keV spectral slopes of the *ASCA* AGN identified in this analysis are inconclusive and improved X-ray observations are required for a more accurate estimate of the 2-10 keV spectral indecies of these objects. Better optical spectroscopy is also required to identify the true nature of the narrow-emission-line galaxies.

Finally, more faint and more high redshift $z > 2$ AGN need to be identified in the hard X-ray bands (> 2 keV). This will give a better estimate of the AGN LF in regions of luminosity-redshift space where there is currently little information, and enable more accurate estimates of the AGN contribution to the hard XRB to be made based on the extrapolation of the AGN LF and its evolution with redshift.

ACKNOWLEDGEMENTS

Optical spectroscopy was carried out with the Anglo-Australian Telescope, based on initial identifications of candidates obtained from APM measurements of UK Scmhidt telescope plates. We would like to thank Karl Glazebrook and Frank Freeman for providing excellent assistance during the AAT run. We would also like to thank the referee, Xavier Barcons and Maite Ceballos for drawing our attention to the LMA sample, and supplying appropriate data from that sample. We thank Bruce Grossan for providing a copy of his thesis. We are also indebted to Elihu Boldt for pointing out a numerical error in an earlier version of this paper. KFG acknowledges the receipt of a PPARC studentship.

REFERENCES

Almaini, O., 1996, Ph.D. thesis, University of Durham
Avni Y. Bahcall J.N. 1980, ApJ, 235, 694
Baldwin J.A., Phillips M.M., Terlevich R.J., 1981, PASP, 93, 5
Barcons X., Franceschini A., De Zotti G., Danese L., Miyati T., 1995, ApJ, 455, 480
Boldt E., Leiter D., 1994, in Bicknell G.V., Dopita M.A., Quinn P.J., eds, ASP Conf. Ser. 54, The Physics of Active Galaxies, Astron. Soc. Pac., San Francisco, p131
Bower R.G. et al. 1996, MNRAS, 281, 59
Boyle B.J., 1996, Observatory, 116, 11
Boyle B.J., Shanks T., Peterson B.A., 1988, MNRAS, 235, 935
Boyle B.J., Staveley-Smith L., Stewart G.C., Georgantopoulos I., Shanks T., Griffiths R.E., 1993, MNRAS, 265, 501
Boyle B.J., Griffiths R.E., Shanks T., Stewart G.C., Georgantopoulos I., 1994, MNRAS, 271, 639
Boyle B.J., McMahon R.G., Wilkes B.J., Elvis M., 1995, MNRAS, 276, 315
Carballo R., Warwick R.S., Barcons X., Gonzalez-Serrano J.I., Barber C.R., Martinez-Gonzalez E., Perez-Fournon I., Burgos J., 1995, MNRAS, 277, 1312
Ceballos M.T., Barcons, X. 1996, MNRAS, 282, 493
Chen L.-W., Fabian A.C., Gendreau K.C., 1996, MNRAS, in press
Comastri A., Setti G., Zamorani G., Hasinger G., 1995, A&A, 296, 1
Couch W.J., Shanks T., Pence, W.N., 1985, MNRAS, 213, 215
Fabian A.C., Barcons X., 1992, ARAA, 30, 429
Gendreau et al. 1995, PASJ, 47, L5
Georgantopoulos I., Stewart G.C., Shanks T., Boyle B.J., Griffiths R.E., 1996, MNRAS, 280, 276
Georgantopoulos I., Stewart G.C., Blair A.J., Shanks T., Griffiths R.E., Boyle B.J., Almaini O., Roche N., 1997, in press (Paper I)
Grossan B.A., 1992, PhD thesis, MIT
Hasinger G., Burg R., Giacconi R., Hartner G., Schmidt M., Trumper J., Zamorani G., 1993, AA, 275, 1
Maccacaro T., Della Ceca R., Gioia I.M., Morris S.L., Stocke J.T., Wolter A., 1991, ApJ, 374, 117
Madau P., Ghisellini, G., Fabian A.C., 1994, MNRAS, 270, L17
Metcalfe N., Shanks T., Fong R., Jones L.R., 1991, MNRAS, 249, 498
Mushotsky R.F., 1982, Adv. Space Res., 3, 10

Nandra K., Pounds K.A., 1994, MNRAS, 268, 405
Persic M., De Zotti G., Danese L., Palumbo G.G.C., Franceschini A., Boldt E.A., Marshall F.E. 1989, ApJ, 344, 125
Peterson B.A., Ellis R.S., Efstathiou G., Shanks T., Bean A.J., Fong R., Zen-Long Z., 1986, MNRAS, 221, 233
Piccinotti G., Mushotzky R.F., Boldt E.A., Holt S.S., Marshall F.E., Serlemitsos P.J., Shafer R.A., 1982, ApJ, 253, 485
Pounds K.A., Nandra K, Stewart G.C., George I.M., Fabian A.C., 1990, Nat, 344, 132
Remillard R.A., Bradt H.V., Buckley D.A.H., Roberts W., Schwarz D.A., Tuohy I.R., Wood K., 1986, ApJ, 301, 742
Schade D., Crampton D., Hammer F., Le Fevre O., Lilly S.J., 1996, MNRAS, 278, 95
Shanks T., Geogantopoulos I., Stewart G.C., Pounds K.A., Boyle B.J., Griffiths R.E., 1991, Nat, 353, 315
Tresse L., Rola C., Hammer F., Stasinska G., Le Fevre O., Lilly S.J., Crampton D., 1996, MNRAS, 281, 847
Tucker W.H., Schwarz D.A., 1986, ApJ, 308, 53.
Wilkes B.J., Elvis M., 1987, ApJ, 323, 243
Wood K.S. et al. 1984, ApJS, 56, 507

This paper has been produced using the Blackwell Scientific Publications TEX macros.